Materials Research. 2017; 20(Suppl. 2): 836-841
DOI: http://dx.doi.org/10.1590/1980-5373-MR-2017-0094

Laser Cladding of Fe-based Metallic Glass/MoS_2 Self-lubricating Composites: Effect of Power and Scanning Speed

Giovana Giroto[a], Piter Gargarella[a]*, Rudimar Riva[b], Claudio Shyinti Kiminami[a],

Marcos Fernandes de Carvalho[a], Conrado Ramos Moreira Afonso[a]

[a]Departamento de Engenharia de Materiais (DEMa), Universidade Federal de São Carlos,Rodovia Washington Luís, Km 245,CEP 13565-905, São Carlos, SP, Brazil
[b]Instituto de Estudos Avançados (IEAv), Trevo Coronel Aviador José Alberto Albano do Amarante, n°1, CEP 12228-001, São José dos Campos, SP, Brazil

Received: January 17, 2017; Revised: December 09, 2017; Accepted: December 11, 2017

MoS_2 powder has been used to form "self-lubricating" composite coatings, which are very useful to increase the lifetime of machines where liquid lubricants cannot be used. In this work, amorphous overspray powder of $Fe_{60}Cr_8Nb_8B_{24}$ (at%) alloy was mixed with 5wt.% MoS_2 powder and it was used to produce single tracks on AISI 1020 steel substrates by laser cladding. The tracks were characterized by X-ray diffraction (XRD), scanning electron microscopy (SEM), differential scanning calorimetry (DSC) and Vickers microhardness. It was observed α-Fe, an Nb-rich intermetallic and MoS_2 particles in the tracks, regardless of laser parameter used. DSC analyses proved the presence of amorphous phase for samples produced with parameters 200W/33.3mm/s, 600W/100mm/s, 800W/100mm/s and 800W/150mm/s. The tracks produced with larger power (800W) and higher scanning speeds (100 and 150mm/s) exhibited a better integrity and homogeneity, lower dilution and presence of amorphous phase, being these parameters considered the most appropriate to produce composite coatings of $Fe_{60}Cr_8Nb_8B_{24}$ (at%)/5wt% MoS_2containing amorphous phase. Hardness tests showed that the single tracks produced are harder than the substrate, for example, the track produced with 800W/150mm/s exhibits hardness six times higher than the steel substrate, 1200 $HV_{0.3}$ and 200 $HV_{0.3}$, respectively.

Keywords: *Laser cladding, metallic glass, self-lubricating composites, Fe-based alloy.*

1. Introduction

Fe-based bulk metallic glasses (BMG) are promising materials to be used as coatings because they exhibit very high mechanical strength (near theoretical limits) combined with high corrosion resistance[1]. Some obstacles for their wide use in structural applications are their relatively high production cost and low ductility[2]. Cheney and Vechio have prepared Fe-Cr-Nb-B metallic glasses using lower cost raw materials as 430 stainless steel and they showed that these alloys present high glass-forming ability (GFA), with critical casting thickness for amorphization up to 3.6 mm[2]. The $Fe_{60}Cr_8Nb_8B_{24}$ alloy belongs to this family and apart from its high GFA, it exhibits high hardness (>1000 HV) and a higher corrosion resistance[3].

Several methods have been used to prepare glassy or amorphous metallic coatings including laser cladding[4], low or high velocity oxygen-fuel spraying (LVOF and HVOF, respectively)[3] and spray forming[3]. Although still more expensive than the other methods, laser cladding has several advantages as: high cooling rate during solidification, low solute segregation, very small heat-affected zone, and fast processing speed with good repeatability and adaptability to automation[5].

A new class of coatings has been created with the incorporation of dry lubricants particles as MoS_2, forming composite coatings so-called self-lubricating coatings[6]. These coatings allow increasing the lifetime of tools and machines where liquid lubricants cannot be used. A problem appears when the MoS_2 is sintered with steels because the high temperatures (1150 and 1350°C) and long sintering times make the MoS_2 transforms to FeS, which does not have the self-lubricating properties. The laser cladding process may be an alternative to prepare $Fe_{60}Cr_8Nb_8B_{24}/MoS_2$ coatings because the interaction time with the laser beam may be short enough to prevent the decomposition of the MoS_2, which may allow to prepare $Fe_{60}Cr_8Nb_8B_{24}/MoS_2$ coatings with good corrosion resistance, high hardness and low friction coefficient because the presence of MoS_2.

It should be noted that several important technological aspects remain to be fully understood during preparation of $Fe_{60}Cr_8Nb_8B_{24}/MoS_2$ self-lubrificating coatings as the MoS_2 thermal stability during processing and the influence of dilution, i.e. changes of coating composition with the partial melting of the substrate. Considering this, the aim of this work is to produce single tracks of $Fe_{60}Cr_8Nb_8B_{24}/MoS_2$ using different laser powers and laser scanning speeds

*e-mail: piter@ufscar.br

to investigate their influence in the microstructure, phase formation and mechanical properties.

2. Experimental

The $Fe_{60}Cr_8Nb_8B_{24}$ (at%) alloy used in this work was spray formed following a similar procedure found in literature[7-10] in an induction melting furnace using as raw materials a ferritic stainless steel (FSS) AISI 430 with 13% Cr content, combined with additions of Fe-67%Nb and Fe-14%B (wt%) alloys. This alloy was processed by a spray forming process using nitrogen (N_2) as the atomization gas, the powder was collected from the bottom of the atomization chamber and sieved and separated into several granulometric size ranges. For this study, powders with a size range greater than 45 μm were milled using high-energy ball milling to decrease the particle size to the range of < 45 μm, using a mill Zoz (Simoloyer CM08). Then, this powder was manually mixed with 5 wt% self-lubricating powder (MoS_2), which presents particle size of 3 μm. This amount of MoS_2 was chosen in order to have perfect powder flowability and do not considerable change the alloy composition.

Laser cladding was carried out by the pre-placed powder method using the ball milling powder mixed with MoS_2, in order to produce single tracks on AISI 1020 mild steel. The single tracks were prepared by placing a 0.2 mm thick layer on the AISI 1020 substrate. These layers were clad using different laser powers (200, 400, 600 and 800 W) and scanning speeds (150, 100, 66.7, 33.3 and 16.6 mm/s), which resulted in a variation of the energy density from 7 to 240 J/mm^2. These parameters were chosen considering a previous work with the $Fe_{60}Cr_8Nb_8B_{24}$ (at%) alloy[11]. The five scanning speeds were used in combination with each power to prepare twenty different single tracks. The aim was to select parameters that allowed amorphous and/or nanocrystalline phase formation with minimal dilution while still creating a metallurgical bonding with the steel substrate and to characterize the microstructure, phase formation, thermal stability and microhardness of the samples. Laser cladding experiments were conducted with a IPG YLM 2000S Yb Fiber Laser (up to 2kW) on the air. The laser beam presented a near Gaussian profile and its diameter on sample surface was 1 mm.The microstructure of the single tracks was analyzed by scanning electron microscopy (SEM) with a FEI Inspect S50. The phases formed in the single tracks were analyzed by X-ray diffraction (XRD) using a Siemens D5005 diffractometer and Cu-K_α radiation. The thermal stability was examined by differential scanning calorimetry (DSC) using a calorimeter DSC Netzsch 404 under a heating rate of 20 K/min.The DSC analyses were carried out for only 7 single tracks produced using laser power and scanning speed of 200 W/33.3 mm/s, 400W/33.3 mm/s, 400W/66.6 mm/s, 600W/66.66 mm/s, 600W/100 mm/s, 800W/100 mm/s and 800W/150 mm/s.The other samples were not analyzed because: i) the tracks were too irregular and were disregarded or ii) because the mass was not enough for the DSC analyses (minimum around 10 mg). The microhardness of the single tracks was measured with a HMV-2000 SHIMADZU microhardness tester and a Vickers pyramid-shaped diamond indenter, under different loads from 0.3 (300 g) up to 1 kg and 15 s of loading.

3. Results and Discussion

Figure 1 shows SEM images (BSE mode) of the $Fe_{60}Cr_8Nb_8B_{24}$ (at%) +5wt% MoS_2 single tracks cross section produced by pre-placed laser cladding using different parameters. Due to the similarity of some results, just a few representative micrographs are shown. The scanning speed and laser power used were 200 W with 33.3 and 100 mm/s, 400 W with 150 mm/s and 800 W with 150 mm/s for the tracks shown in figures 1(a) to 1(d), respectively.

Figures 1 (a) and 1(b) depict the $Fe_{60}Cr_8Nb_8B_{24}$ (at%) +5wt% MoS_2 single tracks produced with laser power of 200 W and scanning speeds of 33.3 and 100 mm/s, respectively. These micrographs show that decreasing the laser scanning speed, a larger penetration depth is observed as a result of the larger energy input. Similar behavior was observed for tracks prepared with other laser powers: 400, 600 and 800 W. The energy input, E_L , is calculated using equation[12]:

$$E_L = \frac{P_L}{(v_s \cdot l_z)} \quad (1)$$

where P_L is the laser power, v_s the scanning speed and l_z is the layer thickness. This equation demonstrates that larger power and smaller scanning speed leads to larger energy input, which may cause a larger penetration depth, i.e. larger dilution. It affects the coating composition and its properties. Considering that the substrate is an AISI 1020 steel, it contains mainly Fe. A higher dilution may add more Fe to the $Fe_{60}Cr_8Nb_8B_{24}$ (at%) composition, which tends to decrease the glass-forming ability of this alloy[2,13].

Figures 1(b) and 1(c) give examples of single tracks with different types of defects, i.e. absence of metallurgical bonding and presence of cracks and big pores. The presence of big pores was, probably, due to imprisonment of gas released during heating of the MoS_2 (reaction of oxidation) as will be discussed later.The crack arises from the high residual stresses stored during processing and absence of a good metallurgical bonding with the substrate.

The heat-affected zone varied from 100 to 250 μm (Figure 1) depending on processing parameters. Usually, high-energy input promotes a larger heat-affected zone.

Figure 1(e) depicts a magnification of the 200 W/ 33.3 mm/s single track (cross section). Spherical morphology particles can be seen in a dark matrix together with brighter elongated precipitates. The EDS maps taken from this track (Figures 1(f) to 1(h)) show that the darker spherical particles

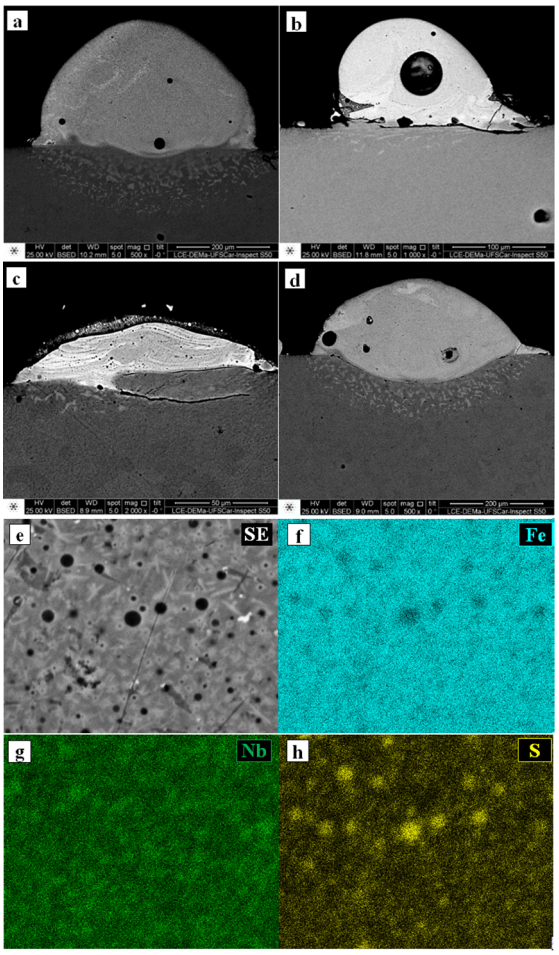

Figure 1. SEM images (BSE mode) of the $Fe_{60}Cr_8Nb_8B_{24}$ (at%) + 5wt% MoS_2 single tracks produced by laser cladding on AISI 120 steel, using different scanning speeds and laser powers: (a) 33.3 mm/s and 200 W, (b) 100 mm/s and 200 W, (c) 150 mm/s and 400 Wand (d) 150 mm/s and 800 W.(e) SEM image in higher magnification of (a) and respective X-ray elemental maps through EDS of (f) Fe-K, (g) Nb-L and (h) S-K related to MoS_2 phase.

correspond to the MoS_2 and the brighter precipitates are an Nb-rich intermetallic. The matrix correspond to α-Fe dendrites. It was not possible to measure the composition of phases or coating because B and S cannot be correctly quantified by the EDS used.

To confirm these results, XRD measurements were carried out at the top surface of the single tracks. The measurements were performed only in some single tracks (200 W with 33.3 mm/s; 400 W with 33.3 and 66.7 mm/s; 600 W with 16.6, 66.7 and 100 mm/s and 800 W with 16.6, 100 and 150 mm/s) and the XRD results are shown in figure 2. Sharp and broad peaks were observed and they correspond to the α-Fe and MoS_2 phases. No clear presence of amorphous phase or Nb-rich intermetallic could be inferred from the XRD results, which is related with their low volume fraction.

It was observed that the tracks produced with larger power (800 W, figure 1(d)) exhibited a lower amount of

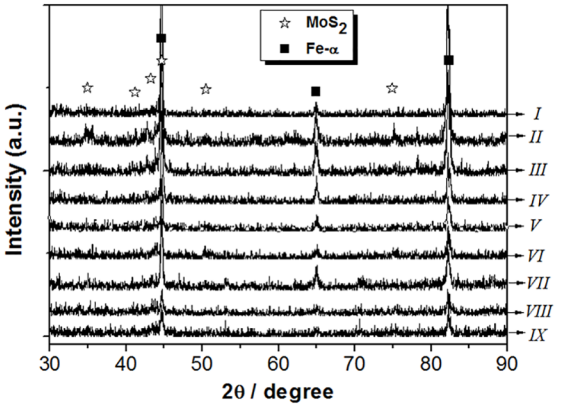

Figure 2. X-ray diffraction patterns of the $Fe_{60}Cr_8Nb_8B_{24}$ (at%) + 5wt% MoS_2 single tracks produced with laser powers and scanning speeds: 200 W with 33.3 mm/s (IX); 400 W with 33.3 (VII) and 66.7 mm/s (VIII); 600 W with 16.6 (III), 66.7 (I) and 100 mm/s (VI) and 800 W with 16.6 (II), 100 (IV) and 150 mm/s (V).

defects (cracks and pores), showed a good metallurgical bonding with the substrate and have a more homogeneous track when compared with the other tracks. Apart from these characteristics, it also desirable the presence of the glassy or amorphous phase in the single tracks. To form this phase in the coatings, a high cooling rate must be applied during solidification. The cooling rate during laser processing can be estimated by the equation below proposed by Ashby and Easterling for a moving line source[14]:

$$\frac{\partial T}{\partial t} = -2\pi k\left[\frac{v}{\alpha q^*}\right](T - T_0)^2 \text{ and } q^* = q - 2r_b z_m v L \quad (2)$$

where k is the thermal conductivity, α is the absorptivity at the sample surface, q is the laser power used, v is the scanning speed, $(T- T_0)$ is the difference between room and melting temperature, r_b is the laser beam radius, z_m is the melt depth and L is the latent heat of melting. It shows that higher scanning speeds and lower powers promotes a higher cooling rate, which allows forming more amorphous or glassy phase in the coatings.

In order to prove the presence of the amorphous phase, DSC measurements were carried out. As mentioned before, the DSC analyses were made for only 7 single tracks produced using laser power and scanning speed of 200 W/33.3 mm/s, 400W/33.3 mm/s, 400W/66.6 mm/s, 600W/66.66 mm/s, 600W/100 mm/s, 800W/100 mm/s and 800W/150 mm/s. The results are shown in figure 3, which depicts the DSC curve of $Fe_{60}Cr_8Nb_8B_{24}$ (at%) + 5wt% MoS_2 single track produced using scanning speed of 100 mm/s and laser power of 800 W. Similar curves were also seen for single tracks produced with 200 W/33.3 mm/s, 600W/100 mm/s and 800W/150 mm/s (not show here).

It can be seen in Figure 3 that the DSC curve indicates three transformations: the first around 500 °C, is exothermic and is related to the MoS_2 transformation; the second at 620 °C is related to the amorphous phase crystallization;

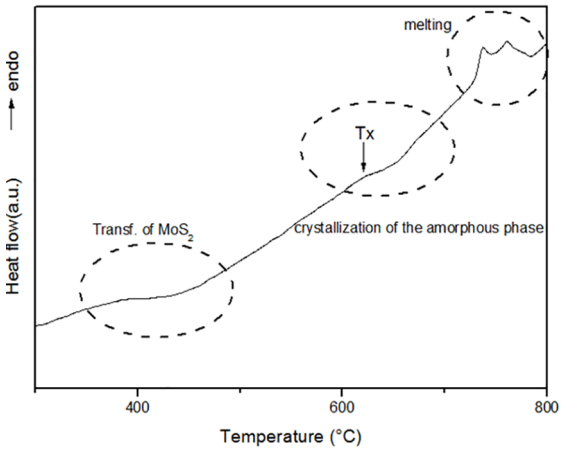

Figure 3. DSC curve of the $Fe_{60}Cr_8Nb_8B_{24}$ (at%) + 5wt% MoS_2 single track, produced using scanning speed of 100 mm/s and laser power of 800 W. The oxidation of the MoS_2, crystallization and melting process are shown by dashed lines. T_x means crystallization temperature.

and the third, between 704 and 780 °C, is related to the melting process. The first transformation corresponds to the thermic oxidation of MoS_2, which is transformed to MoS_3. This oxidation process enhances as the temperature increases. Around 10%, 50% and 90% of MoS_3 are formed at temperatures of 435 °C, 466 °C and 516 °C, respectively, when the MoS_2 is exposed to dry air[15]. The size of the MoS_2 particles also influence, significantly, in the oxidation rate, since small particles have a much higher oxidation rate. Considering that the MoS_2 particles have a size of 3µm, the thermic oxidation was favored due to this small particle size.

The second exothermic peak in the DSC curve (Figure 3) represents the crystallization of the amorphous phase formed in the coating. The onset crystallization temperature was 620 °C. Koga et. al[16] studied a $Fe_{60}Cr_8Nb_8B_{24}$(at%) glassy ribbon and observed that the glass transition temperature (T_g) and the crystallization temperature (T_x) are 606°C and 660 °C, respectively. The presence of crystals and MoS_2 caused changes in the chemical composition of the amorphous phase, which explains the change in the crystallization temperature when compared with Koga et al. Only four single tracks exhibited crystallization peaks (i.e. formed amorphous phase): the tracks produced using 200 W/33.3 mm/s, 600W/100 mm/s, 800W/100 mm/s and 800W/150 mm/s. It is expected that more amorphous phase forms in samples prepared under higher cooling rates. We estimated the cooling rates using equation 2 and the values are given in Table 1. The calculation was carried out considering laser beam radius of 0.5 mm, thermal conductivity of 43 W/mK, absorptivity of 0.2, latent heat of melting of 272 KJ/Kg and (T - T_0) of 755 K. The lower cooling rates were calculated for 400W/33.3 mm/s and 600W/66.66 mm/s and they may explain why amorphous phase was not formed in these samples. Nevertheless, the 400W/66.6 mm/s sample solidified under a cooling rate similar to the other samples and it should form amorphous phase. The reason for this apparent contradiction is not clear. It may be related with a low amount of amorphous phase presented in the sample, which could not be detected by DSC.

Table 1. Calculated cooling rates for the samples investigated by DSC.

Sample	Cooling rate (K/s)	Was amorphous phase detected?
200 W/33.3 mm/s	-128207.6	Yes
400W/33.3 mm/s	-64103.8	No
400W/66.6 mm/s	-128400.1	No
600W/66.66 mm/s	-85600.0	No
600W/100 mm/s,	-128335.9	Yes
800W/100 mm/s	-96251.9	Yes
800W/150 mm/s	-144377.9	Yes

The mechanical properties of the single tracks produced were estimated by microhardness measurements. Microhardness profiles taken from top of some coatings to the substrate are shown in Figures 4(a) and 4(b). Comparing the different single tracks, it can be observed that the average microhardness values varied between 500 HV and 1200 HV, depending on the scanning speed. As expected, it can be seen that the microhardness values decrease from the top to the substrate, irrespective of parameters used. Comparing the results, the single track prepared using 800W/150 mm/s exhibits the highest hardness around 1200 HV0.3. It may be related with the amount and distribution of the amorphous phase in this coating, which increases the hardness and strength. Comparing coatings prepared with the same power, it can be seen that higher scanning speeds give rise to higher hardness values as expected because of the high cooling rate applied, which promotes microstructural refinement and formation of more amorphous phase.

These results attest the coatings of $Fe_{60}Cr_8Nb_8B_{24}$ (at%) +5 wt% MoS_2 have higher hardness when compared with the AISI 1020 substrate. As one example, the single track produced using 800 W and 150 mm/s (figure 1(f)) exhibits a hardness around 1200 HV0.3, six times higher than the substrate (200 HV0.3). The hardness obtained for this coating is comparable with the hardness observed for a WC-12%Co coating obtained by thermal spraying (hardness around 1200 HV0.3[17]), nevertheless, a lower friction coefficient is expected as a result of the MoS_2 presence. Considering the high hardness and strength and the presence of the dry lubrificant MoS_2, it is expected that the single tracks exhibit an excellent wear behaviour with a great potential to be used as protective coatings of steel substrates. More corrosion and wear tests should be carried out in larger coatings in order to validate these results. It is expected that the presence of α-Fe crystals in the glass may deteriorates the corrosion resistance

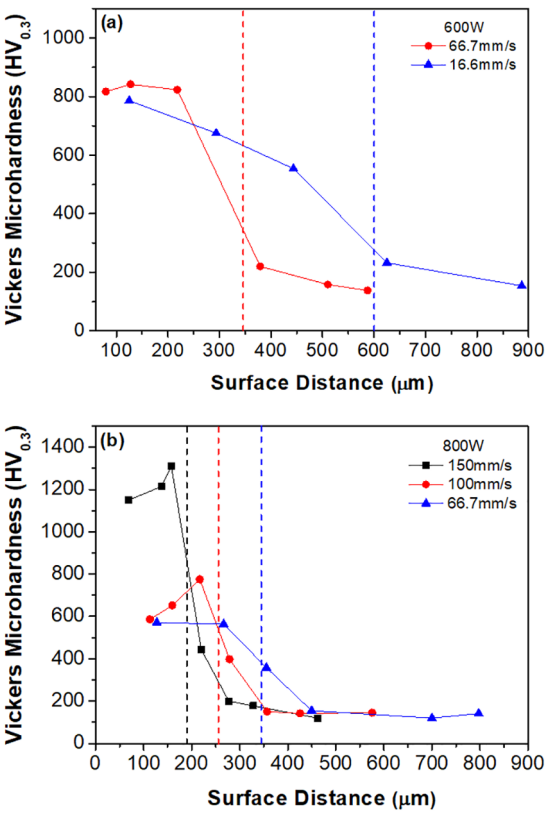

Figure 4. Vickers microhardness profiles of cross sections of the $Fe_{60}Cr_8Nb_8B_{24}$ (at%) + 5wt% MoS_2 single tracks obtained using (a) 600W and (b) 800W. The scanning speeds used are indicate in the figures.The dashed lines indicated the thickness of the coating in each case.

of the coatings because the presence of a galvanic cell with Fe-α acting as anode and the amorphous matrix as cathode.

4. Conclusions

All tracks exhibited micrometric α-Fe grains and MoS_2 particles together with a Nb-rich intermetallic, regardless of laser parameters used. Amorphous phase was detected only in some tracks produced with 200 W/33.3 mm/s, 600W/100 mm/s, 800W/100 mm/s and 800W/150 mm/s. The single tracks produced with larger power (800W) and higher scanning speeds (100 and 150 mm/s) exhibited a lower amount of defects, a better integrity and homogeneity, lower dilution and presence of amorphous phase and because of these reasons, these parameters are the most appropriate to produce composite coatings of $Fe_{60}Cr_8Nb_8B_{24}$ (at%)/5 wt% MoS_2 containing amorphous phase. The hardness tests showed that the single tracks are harder than the substrate, with hardness six times higher than the steel substrate for the single track produced with 800W/150 mm/s.

5. Acknowledgments

The authors would like to thank the institutions: FAPESP (São Paulo Research Foundation) for the "Projeto Temático" #2013/05987-8; "Projeto Regular" #2012/18429-0; Post-Doctorate Grant #2014/13432-9 and #2015/04062-6 and the Ministry of Science and Technology (MCT) "PRONEX" for the financial support and to the Structural Characterization Laboratory (LCE) by the FRX, SEM, EDS and XRD analysis.

6. References

1. Suryanarayana C, Inoue A. *Bulk Metallic Glasses*. Boca Raton: CRC Press; 2011.
2. Cheney J, Vecchio K. Development of quaternary Fe-based bulk metallic glasses. *Materials Science and Engineering: A*. 2008;492(1-2):230-235.
3. Melle AK. *Produção e caracterização de recobrimentos de aço, empregando a liga amorfizável Fe-Cr-Nb-B*. [Dissertation]. São Carlos: Universidade Federal de São Carlos; 2012.
4. Gargarella P, Almeida A, Vilar R, Afonso CRM, Peripolli S, Rios CT, et al. Formation of Fe-based glassy matrix composite coatings by laser processing. *Surface and Coatings Technology*. 2014;240:336-343.
5. Vilar R. Laser cladding. *Journal of Laser Applications*. 1999;11(2):64-79.
6. Sliney HE. The Use of Silver in Self-Lubricating Coatings for Extreme Temperatures. *A S L E Transactions*. 1986;29(3):370-376.
7. Afonso CRM, Bolfarini C, Botta Filho WJ, Kiminami CS. Spray forming of the glass former $Fe_{83}Zr_{3.5}Nb_{3.5}B_9Cu_1$ alloy. *Materials Science and Engineering: A*. 2004;375-377:571-576.
8. Afonso CRM, Bolfarini C, Botta Filho WJ, Kiminami CS. Spray forming of glass former $Fe_{63}Nb_{10}Al_4Si_3B_{20}$ alloy. *Materials Science and Engineering: A*. 2007;449-451:884-889.
9. Rios CT, Afonso CRM, Bolfarini C, Botta Filho WJ, Kiminami CS. Characterization of Glass Forming Alloy $Fe_{43.2}Co_{28.8}B_{19.2}Si_{4.8}Nb_4$ Processed by Spray Forming and Wedge Mold Casting Techniques. *Materials Science Forum*. 2011;691:23-26.
10. Afonso CRM, Kaufman MJ, Bolfarini C, Botta Filho WJ, Kiminami CS. Gas Atomization of Nanocrystalline $Fe_{63}Nb_{10}Al_4Si_3B_{20}$ Alloy. *Journal of Metastable and Nanocrystalline Materials*. 2004;20-21:175-182.
11. Carvalho MF, Riva R, Batista Fogagnolo J, Kiminami CS, Afonso CRM. Metallic Glass Formation Upon Rapid Solidification of $Fe_{60}Cr_8Nb_8B_{24}$ (at%) Alloy through LASER Cladding and Remelting. *Materials Research*. 2017. In press.
12. Gustmann T, Neves A, Kühn U, Gargarella P, Kiminami CS, Bolfarini C, et al. Influence of processing parameters on the fabrication of a Cu-Al-Ni-Mn shape-memory alloy by selective laser melting. *Additive Manufacturing*. 2016;11:23-31.

13. Cheney J, Vecchio K. Evaluation of glass-forming ability in metals using multi-model techniques. *Journal of Alloys and Compounds*. 2009;471(1-2):222-240.

14. Ashby MF, Easterling KE. The transformation hardening of steel surfaces by laser beams-I. Hypo-eutectoid steels. *Acta Metallurgica*. 1984;32(11):935-1937, 1939-1948.

15. Lavik MT, Medved TM, Moore GD. Oxidation Characteristics of MoS_2 and Other Solid Lubricants. *A S L E Transactions*. 1968;11(1):44-55.

16. Koga GY, Nogueira RP, Roche V, Yavari AR, Melle AK, Gallego J, et al. Corrosion properties of Fe-Cr-Nb-B amorphous alloys and coatings. *Surface and Coatings Technology*. 2014;254:238-243.

17. Factor M, Roman I. Vickers microindentation of WC-12%Co thermal spray coating: Part 1: statistical analysis of microhardness data. *Surface and Coatings Technology*. 2000;132(1-2):181-193.